Westre, T.E. et al. Determination of the Fe-N-O angle in {FeNO}7 complexes using multiple-scattering EXAFS Analysis by GNXAS.J. Amer. Chem. Soc. 116, 6757–6768

ARTICLE *in* JOURNAL OF THE AMERICAN CHEMICAL SOCIETY · JULY 1994

Impact Factor: 12.11 · DOI: 10.1021/ja00094a035

Determination of the Fe–N–O Angle in {FeNO}^{7} Complexes Using Multiple-Scattering EXAFS Analysis by GNXAS

Tami E. Westre,[†] Andrea Di Cicco,[‡] Adriano Filipponi,[§] Calogero R. Natoli,[⊥] Britt Hedman,[†,∥] Edward I. Solomon,[†] and Keith O. Hodgson[†,∥]

Contributions from the Dipartimento di Matematica e Fisica, Università degli Studi di Camerino, Via Madonna delle Carceri, 62032 Camerino (MC), Italy, Dipartimento di Fisica, Università degli Studi dell' Aquila, Via Vetoio, 67010 Coppito, L'Aquila, Italy, INFN, Laboratori Nazionali di Frascati, C.P. 13, 00044 Frascati, Italy, and Department of Chemistry and Stanford Synchrotron Radiation Laboratory, Stanford University, Stanford, California 94305

Received January 10, 1994[⊕]

Abstract: The Fe–N–O bond angle in a series of {FeNO}^{7} complexes has been probed by EXAFS, utilizing a new theoretical data analysis package, GNXAS. This package provides an integrated approach to the analysis of EXAFS data based on a full curved-wave, multiple-scattering theoretical treatment incorporating least-squares refinement. Since GNXAS is able to calculate all the signals relating to two-, three-, and four-atom correlation functions with the proper treatment of correlated distances and Debye–Waller factors, it is particularly well-suited for analysis of multiple-scattering effects and bond angle determination. EXAFS data were obtained on a series of crystallographically-characterized {FeNO}^{7} inorganic complexes with varying Fe–N–O angles to examine the sensitivity of the GNXAS fit to this angle. The compounds studied were Fe(TMC)NO (where TMC = 1,4,8,11-tetramethyl-1,4,8,11-tetraazacyclotetradecane) which has an Fe–N–O bond angle of 177.5(5)°, Fe(TACN)$(N_3)_2$NO (where TACN = *N,N',N''*-trimethyl-1,4,7-triazacyclononane) which has an angle of 156(1)°, and Fe(salen)NO (where salen = *N,N'*-ethylenebis(salicylideneiminato)) which has a bond angle of 127(6)° at 175 °C and 147(5)° at 23 °C. EXAFS data for FeEDTA-NO (whose crystal structure has not been determined and thus the angle is unknown) were also obtained and analyzed using GNXAS to determine the Fe–N–O bond angle. Results are presented which indicate that it is possible to determine whether the Fe–N–O unit is bent or linear, with the GNXAS analysis being extremely sensitive when the angle is between 150° and 180°. Using this method the Fe–N–O angle in FeEDTA–NO is found to be 156(5)°. The results of this study establish that EXAFS analysis using GNXAS can provide reliable angular information for small molecules coordinated to transition metals with rather complex coordination environments. This study thus provides the basis for the determination of the coordination geometry of molecules like NO and O_2 to metalloprotein active sites.

Introduction

Mononuclear high-spin non-heme ferrous centers are present in the catalytic active sites of a large number of enzymes involved in the binding and activation of molecular dioxygen.[1] An understanding of the reactivity of these enzymes requires knowledge of the geometric and electronic structures of the active sites as well as their interactions with substrate, dioxygen, and other molecules of relevance to catalysis. Understanding the oxygen intermediates involved in catalysis is key to obtaining molecular insight into the mechanism of the reaction. Unfortunately, these intermediates are often too unstable to allow detailed spectroscopic study. Nitric oxide reversibly binds to the ferrous active site of the native form of many of these non-heme iron enzymes to generate stable nitrosyl complexes.[2] These enzyme–NO complexes can serve as analogs of the possible dioxygen intermediates involved in catalysis and can be readily studied spectroscopically to determine geometric and electronic structure differences which could provide insight into differences in oxygen activation by the enzymes.

However, in order to use the NO derivative of these non-heme iron enzymes as a probe of electron distribution related to dioxygen reactivity, detailed understanding of the electronic and geometric structure of the {FeNO}^{7} unit[3] is required. {FeNO}^{7} complexes have been described in the literature as having different electronic structures for different geometric structures, linear Fe–N–O being viewed as Fe^+ and NO^+ and bent Fe–N–O as Fe^{3+} and NO^-. Enzyme–NO complexes as well as several {FeNO}^{7} model compounds (in particular FeEDTA-NO, *vide infra*) exhibit an unusual $S = {}^3/_2$ EPR signal.[2] A wide range of bonding descriptions have appeared[4] to describe this $S = {}^3/_2$ signal including [Fe^+d^7-($S={}^3/_2$) – $NO^+(S=0)$], [$Fe^{2+}d^6(S=2)$ – $NO^0(S={}^1/_2)$] antiferromagnetically coupled, [$Fe^{3+}d^5(S={}^1/_2)$–$NO^-(S=1)$] ferromagnetically coupled, and [$Fe^{3+}d^5(S={}^3/_2)$–$NO^-(S=0)$]. We have recently used a combination of spectroscopic and theoretical

† Stanford University, Department of Chemistry.
‡ Università degli Studi di Camerino.
§ Università degli Studi dell' Aquila.
⊥ INFN.
∥ Stanford Synchrotron Radiation Laboratory.

⊕ Abstract published in *Advance ACS Abstracts,* June 15, 1994.

(1) (a) Solomon, E. I.; Zhang, Y. *Acc. Chem. Res.* **1992**, *25*, 343. (b) Smith, W. L.; Lands, W. E. M. *J. Biol. Chem.* **1972**, *247*, 1038. (c) Kohlmiller, N. A.; Howard, J. B. *J. Biol. Chem.* **1979**, *254*, 7302. (d) Nozaki, M.; Kagamiyama, H.; Hayaishi, O. *Biochem. Z.* **1963**, *338*, 582. (e) Burger, R. M.; Peisach, J.; Blumberg, W. E.; Wittenberg, J. B.; Sausville, E. A.; Horwitz, S. B. *Electron Transport and Oxygen Utilization*; Elsevier: New York, 1982; pp 319–322. (f) Shiman, R. *Folates and Pterins*; Wiley: New York, 1984; Vol. 2, pp 179–249. (g) Lindstedt, S.; Odelhög, B.; Rundgren, M. *Biochemistry* **1977**, *16*, 3369. (h) Ruettinger, R. T.; Griffith, G. R.; Coon, M. J. *Arch. Biochem. Biophys.* **1977**, *183*, 528. (i) Batie, C. J.; LaHaie, E.; Ballou, D. P. *J. Biol. Chem.* **1987**, *262*, 1510. (j) Pang, C. P.; Chakravarti, B.; Adlington, R. M.; Ting, H. H.; White, R. L.; Jayatilake, G. S.; Baldwin, J. E.; Abraham, E. P. *Biochem. J.* **1984**, *222*, 789. (k) Slykhouse, T. O.; Fee, J. A. *J. Biol. Chem.* **1976**, *251*, 5472.

(2) (a) Nelson, M. J. *J. Biol. Chem.* **1987**, *262*, 12137. (b) Rich, P. R.; Salerno, J. C.; Leigh, J. S.; Bonner, W. D. *FEBS Lett.* **1978**, *93*, 323. (c) Arciero, D. M.; Lipscomb, J. D. *J. Biol. Chem.* **1986**, *261*, 2170. (d) Arciero, D. M.; Orville, A. M.; Lipscomb, J. D. *J. Biol. Chem.* **1985**, *260*, 14035. (e) Twilfer, H.; Bernhardt, F.-H.; Gersonde, K. *Eur. J. Biochem.* **1985**, *147*, 171. (f) Chen, V. J.; Orville, A. M.; Harpel, M. R.; Frolik, C. A.; Surerus, K. K.; Münck, E.; Lipscomb, J. D. *J. Biol. Chem.* **1989**, *264*, 21677.

(3) The Feltham–Enemark[3b] formalism for {MNO}^{x} complexes is used here in which x is the number of d type electrons in the system when the nitrosyl ligand is formally considered as NO^+. (b) Enemark, J. H.; Feltham, R. D. *Coord. Chem. Rev.* **1974**, *13*, 339.

0002-7863/94/1516-6757$04.50/0

methods to determine that the appropriate description of the $S = {}^3/_2$ {FeNO}^{7} unit is high-spin $Fe^{3+}(S = {}^5/_2)$ antiferromagnetically coupled to an NO^- ($S=1$) to produce the $S = {}^3/_2$ ground state.[5]

In the present study, extended X-ray absorption fine structure (EXAFS) data on a series of {FeNO}^{7} model compounds were measured and analyzed to characterize the geometric structure of the Fe–N–O unit. Multiple-scattering effects from distant shells can contribute significantly to the EXAFS of inorganic molecules,[6] and these effects have been used in a few favorable cases to obtain angular information.[7] The effects are particularly evident when an intervening atom nears a linear relationship with an absorber and a distant scatterer, as occurs in Fe-oxo dimers[7b] and metal carbonyls.[8] An empirical data-analysis approach was utilized to determine the Fe–O–Fe angle in oxygen-bridged iron complexes.[7b] The analysis demonstrated that it was possible to estimate the Fe–O–Fe bridging angle to within ±8° and calculate the Fe–Fe distance to ±0.05 Å. In the present study, the same traditional empirical EXAFS technique was initially applied to the {FeNO}^{7} systems to determine the Fe–N–O angle. However, determination of the Fe–N–O angle using the empirical technique was not found to be possible because the oxygen of the Fe–N–O is not a heavy back-scatterer, the quality of empirical Fe–N and Fe–O (second shell) phases and amplitudes is poor, and other low Z atoms are at approximately the same distance as the Fe–O (second shell).[9] Since angle determination by empirical methods did not prove to be feasible, a new theoretical EXAFS data analysis package, GNXAS,[10] was utilized to probe the Fe–N–O bond angle using a multiple-scattering analysis and establish the generality of the approach for angle determination of low Z small molecules liganded to transition metal complexes.

The GNXAS package provides a new integrated approach to the analysis of EXAFS data based on full curved-wave, multiple-scattering theoretical analysis. It incorporates direct fitting of theoretical spectra (calculated by utilizing the Hedin–Lundqvist complex exchange and correlations potential[11]) to the experimental data and utilizes single- and multiple-scattering signals with the proper treatment of correlated distances and Debye–Waller factors. GNXAS has been evaluated on simpler systems (including SiX_4 (X = F, Cl, CH_3),[12] $Os_3(CO)_{12}$,[8d] Br_2 and HBr,[13] and brominated hydrocarbons[14]) and a more complex heterometal cluster.[15] It has been demonstrated that the GNXAS method can provide accurate bond distances and angles for second and third neighbors for Fe complexes.[16]

In this study, the EXAFS data of a series of crystallography-characterized {FeNO}^{7} compounds with varying Fe–N–O angles were analyzed using the GNXAS method to examine the sensitivity of this method to Fe–N–O angle determination. The compounds studied were $[Fe(TMC)NO](BF_4)_2$[17] (where TMC = 1,4,8,11-tetramethyl-1,4,8,11-tetraazacyclotetradecane), which has an Fe–N–O bond angle of 177.5(5)°, $Fe(TACN)(N_3)_2NO$[4e] (where TACN = *N,N',N''*-trimethyl-1,4,7-triazacyclonane), which has an angle of 156(1)°, and Fe(salen)NO[18] (where salen = *N,N'*-ethylenebis(salicylideneiminato)) which has a bond angle of 127(6)° at −175 °C and 147(5)° at 23 °C.

EXAFS data for FeEDTA-NO (whose crystal structure is not known due to lack of suitable crystals) were obtained and analyzed to determine the unknown Fe–N–O bond angle. In order to use the GNXAS method to calculate the theoretical EXAFS spectrum, an initial structural model is needed. Such a model for this unknown structure was obtained by comparing first shell empirical fits of the EXAFS data of $[Fe(H_2O)EDTA]^-$, $[Fe(H_2O)EDTA]^{2-}$, and FeEDTA-NO. The Fe–O and Fe–N distances of the EDTA ligand in FeEDTA-NO were much closer to the distances in $[Fe(H_2O)EDTA]^-$ than the respective distances in $[Fe(H_2O)EDTA]^{2-}$, consistent with our description of the FeEDTA-NO complex as having a ferric center.[5] Thus bond distances and angles from the crystallographically-characterized $[Fe(H_2O)EDTA]^-$ were used as an initial structural model in the GNXAS analysis with NO substituted for the bound water.[19] Since the EXAFS data for FeEDTA-NO were collected as a frozen solution, EXAFS data were also collected for $Na[Fe(OH_2)EDTA]$ as a solution as well as a powder to determine if the metrical details differed in the two states. The results of this study establish that EXAFS analysis by GNXAS can provide reliable angular information and serve as the basis for its application to NO complexes of non-heme iron protein active sites.

Experimental Section

Sample Preparation and Data Collection. X-ray absorption (XAS) spectra were recorded at the Stanford Synchrotron Radiation Laboratory on unfocused beamlines 7-3 and 4-3 during dedicated conditions (3 GeV, 25–75 mA). The radiation was monochromatized using a Si(220) double-crystal monochromator detuned 50% at 7998 eV to minimize harmonic contamination. An Oxford Instruments continuous-flow liquid helium CF 1208 cryostat was used to maintain a constant temperature. The XAS spectra were calibrated using an internal Fe foil standard,[20] assigning the first inflection point to 7111.2 eV.

$[Fe(TMC)NO](BF_4)_2$,[17] $Fe(TACN)(N_3)_2NO$,[4e] Fe(salen)NO,[18] and $Na[Fe(OH_2)EDTA]$[19] were prepared as described in the literature. $[Fe(TMC)NO](BF_4)_2$, $Fe(TACN)(N_3)_2NO$, and Fe(salen)NO are air-sensitive and were handled in a nitrogen-filled inert atmosphere dry glove box during the following sample preparation. The crystalline samples were mixed with BN and ground into a fine powder. The BN/sample mixture was pressed into a 1 mm thick Al spacer that was sealed with 63.5 μm mylar tape windows. Immediately after preparation, the samples were frozen in liquid nitrogen. Data were measured in transmission mode at 10 K with nitrogen-filled ionization chambers. Since Fe(salen)NO undergoes a spin and structural transition at 180 K, EXAFS data were also collected at 220 K.

(4) (a) Wells, F. V.; McCann, S. W.; Wickman, H. H.; Kessel, S. L.; Hendrickson, D. N.; Feltham, R. D. *Inorg. Chem.* **1982**, *21*, 2306. (b) Bill, E.; Bernhardt, F.-H.; Trautwein, A. X.; Winkler, H. *Eur. J. Biochem.* **1985**, *147*, 177. (c) Earnshaw, A.; King, E. A.; Larkworthy, L. F. *J. Chem. Soc. (A) Inorg. Phys. Theor.* **1969**, 2459. (d) Salerno, J. C.; Siedow, J. N. *Biochem. Biophys. Acta* **1979**, *579*, 246. (e) Pohl, K.; Wieghardt, K.; Nuber, B.; Weiss, J. *J. Chem. Soc., Dalton Trans.* **1987**, 187.

(5) Zhang, Y.; Pavlosky, M. A.; Brown, C. A.; Westre, T. E.; Hedman, B.; Hodgson, K. O.; Solomon, E. I. *J. Am. Chem. Soc.* **1992**, *114*, 9189.

(6) (a) Ashley, C. A.; Doniach, S. *Phys. Rev. B* **1975**, *11*, 1279. (b) Lee, P. A.; Pendry, J. B. *Phys. Rev. B* **1975**, *11*, 2795. (c) Cramer, S. P. Ph.D. Thesis, Stanford University, 1978.

(7) (a) Teo, B.-K. *J. Am. Chem. Soc.* **1981**, *103*, 3990. (b) Co, M. S.; Hendrickson, W. A.; Hodgson, K. O.; Doniach, S. *J. Am. Chem. Soc.* **1983**, *105*, 1144.

(8) (a) Cramer, S. P.; Hodgson, K. O.; Stiefel, E. I.; Newton, W. E. *J. Am. Chem. Soc.* **1978**, *100*, 2748. (b) Binsted, N.; Evans, J.; Greaves, G. N.; Price, R. J. *J. Chem. Soc., Chem. Commun.* **1987**, 1330. (c) Binsted, N.; Cook, S. L.; Evans, J.; Greaves, G. N.; Price, R. J. *J. Am. Chem. Soc.* **1987**, *109*, 3669. (d) Filipponi, A.; Di Cicco, A.; Zanoni, R.; Bellatreccia, M.; Sessa, V.; Dossi, C.; Psaro, R. *Chem. Phys. Lett.* **1991**, *184*, 485.

(9) Westre, T. E.; Hedman, B.; Solomon, E. I.; Hodgson, K. O. Unpublished data.

(10) (a) Filipponi, A.; Di Cicco, A.; Tyson, T. A.; Natoli, C. R. *Solid State Commun.* **1991**, *78*, 265. (b) Filipponi, A.; Di Cicco, A. *Synch. Rad. News* **1992**, *6*, 13.

(11) Hedin, L.; Lundqvist, S. *Solid State Phys.* **1969**, *23*, 1.

(12) Di Cicco, A.; Stizza, S.; Filipponi, A.; Boscherini, F.; Mobilio, S. *J. Phys. B* **1992**, *25*, 2309.

(13) D'Angelo, P.; Di Cicco, A.; Filipponi, A.; Pavel, N. V. *Phys. Rev. A* **1993**, *47*, 2055.

(14) Burattini, E.; D'Angelo, P.; Di Cicco, A.; Filipponi, A.; Pavel, N. V. *J. Phys. Chem.* **1993**, *97*, 5486.

(15) Nordlander, E.; Lee, S. C.; Cen, W.; Wu, Z. Y.; Natoli, C. R.; Di Cicco, A.; Filipponi, A.; Hedman, B.; Hodgson, K. O.; Holm, R. H. *J. Am. Chem. Soc.* **1993**, *115*, 5549.

(16) Westre, T. E.; Di Cicco, A.; Filipponi, A.; Natoli, C. R.; Hedman, B.; Solomon, E. I.; Hodgson, K. O. *J. Am. Chem. Soc.* Submitted for publication.

(17) Hodges, K. D.; Wollman, R. G.; Kessel, S. L.; Hendrickson, D. N.; Van Derveer, D. G.; Barefield, E. K. *J. Am. Chem. Soc.* **1979**, *101*, 906.

(18) Haller, K. J.; Johnson, P. L.; Feltham, R. D.; Enemark, J. H. *Inorg. Chim. Acta* **1979**, *33*, 119.

(19) Lind, M. D.; Hamor, M. J.; Hamor, T. A.; Hoard, J. L. *Inorg. Chem.* **1963**, *3*, 34.

(20) Scott, R. A.; Hahn, J. E.; Doniach, S.; Freeman, H. C.; Hodgson, K. O. *J. Am. Chem. Soc.* **1982**, *104*, 5364.

The $[Fe(OH_2)EDTA]^{2-}$ solution, 50 mM in Fe, was prepared by anaerobically adding ferrous ammonium sulfate to a 50 mM solution of Na_2EDTA in pH = 6.5, 0.1 M deoxygenated phosphate buffer. Oxidizing this solution produced $[Fe(OH_2)EDTA]^-$. An FeEDTA-NO solution was prepared by purging an $[Fe(OH_2)EDTA]^{2-}$ solution with NO gas under anaerobic conditions. To form an ice-free glass, the XAS solution samples were prepared by adding 50% (by volume) glycerol to the previously prepared solutions resulting in solutions 25 mM in Fe. These samples were loaded into 140 μL Lucite EXAFS cells (23 × 2 × 3 mm) with 37 μm Kapton windows in an anaerobic wet box under nitrogen. The samples were frozen in liquid nitrogen and were subsequently stored in a liquid nitrogen refrigerator until use. Data were collected in fluorescence mode at 10 K. The fluorescence signal was collected by an argon-filled ionization chamber,[21] equipped with Soller slits and a Mn filter.

Data were also collected for Fe(acetylacetonate)$_3$ and [Fe(1,10-phenanthroline)$_3$](ClO$_4$)$_3$ at 10 K to extract Fe–O and Fe–N backscattering parameters for empirical analysis. Fe(acetylacetonate)$_3$ was purchased from Aldrich and [Fe(1,10-phenanthroline)$_3$](ClO$_4$)$_3$ was prepared according to the published procedure.[22] The samples were prepared in air in an identical manner to the solids mentioned above. Data were measured in transmission mode with nitrogen-filled ionization chambers.

The EXAFS data were measured to k = 15 Å^{-1} with 2 mm high pre-monochromator beam-defining slits for the $Na[Fe(OH_2)EDTA]$, $Na_2[Fe(OH_2)EDTA]$, and FeEDTA-NO solutions and 1 mm high pre-monochromator slits for all the powder samples. Two to seven scans were averaged for each transmission sample, while eight to twenty scans were averaged for the fluorescence samples. The effects of a quartet monochromator glitch were removed from the averaged data by four single point replacements at around k = 11.8, 12.1, 12.3, and 12.6 Å^{-1}.

GNXAS Data Analysis. As described in detail elsewhere,[10,16] the GNXAS programs generate model EXAFS signals for each shell around the photoabsorber based on an initial structural model. Both single-scattering and multiple-scattering contributions are summed to generate a theoretical spectrum for the model which is then fit to the non-Fourier-filtered experimental data.[10,16]

The crystallographic coordinates were used as input for $[Fe(TMC)NO](BF_4)_2$,[17] $Fe(TACN)(N_3)_2NO$,[4c] and Fe(salen)NO[18] at high and low temperatures (Figure 1 shows the structure of each compound). Phase shifts were calculated using the standard muffin-tin approximation with all the atoms associated with each compound and up to an energy limit of 70 Ry (950 eV) above the Fe K edge. The Mattheiss prescription[23] of overlapping, self-consistent atomic charge densities of the atoms of the cluster was used to construct the Coulomb portion of the effective one-electron potential. Proper account of the charge relaxation around the core hole was taken. The Hedin–Lundqvist plasmon-pole approximation was used to model its exchange and correlation part.[11] The imaginary part of the latter takes into account inelastic scattering processes of the photoelectron propagating out of the system and models *a priori* its mean-free path. The muffin-tin radii were chosen by scaling Norman radii of the cluster atoms by a factor of about 0.8 as to match the nearest neighbor distance.

The theoretical EXAFS spectrum was calculated to include contributions from two-atom and three-atom configurations. Within each n-atom configuration, all the MS contributions were taken into account.[10,16] The two-atom and three-atom configurations were identified in each cluster up to 4.4 Å and averaged with a frequency tolerance of 0.1 Å. The resultant information was used to calculate the various EXAFS $\gamma^{(2)}$ and $\gamma^{(3)}$ signals associated with each two-atom and three-atom contribution using the crystallographic bond lengths and distances.

The GNXAS fitting program constructs the theoretical absorption spectrum by summing all the $\gamma^{(2)}$ and $\gamma^{(3)}$ signals and compares this theoretical spectrum with the experimental absorption spectrum with the residual function R being a measure of the quality of the fit.[16] Least-square fits are performed on the averaged, energy-calibrated, raw absorption data without prior background subtraction or Fourier filtering. Raw data are compared directly with a model absorption coefficient

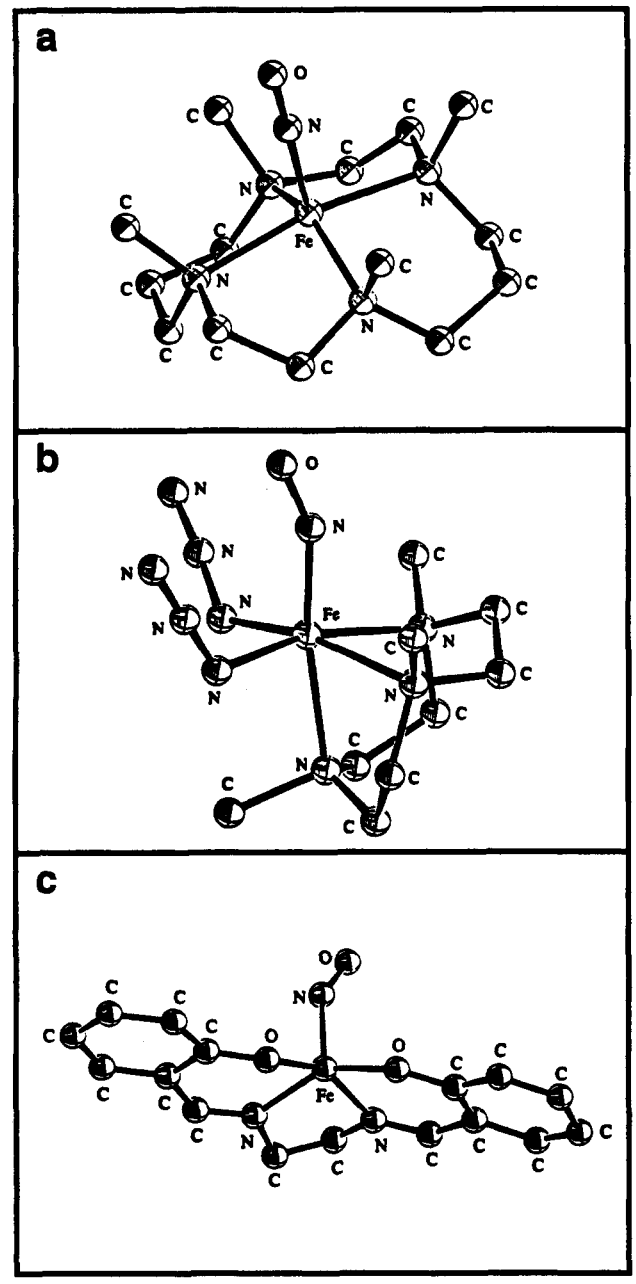

Figure 1. The molecular structure of (a) $[Fe(TMC)NO](BF_4)_2$, (b) $Fe(TACN)(N_3)_2NO$, and (c) Fe(salen)NO at 23 °C.

composed of an appropriate background plus the oscillatory structural contribution from the theoretically calculated EXAFS.[16] A spline of orders 3,4,4 with defining energy points of 7155, 7250, 7600, and 7998 eV was used for most cases. If there was low frequency noise in the Fourier transform (FT) the first defining energy point was adjusted by a maximum of 5 eV until the noise was minimized. Least-squares fits were done with k^3-weighting where the first and the last spline points determined the range of the fit.

The structural parameters varied in the refinements were the distance (R) and the bond variance (σ_R^2), the mean square variation in the bond distance, for each two-atom configuration and the distances, the angle, and the covariance matrix elements[10,16] for the three-atom configurations. Distances and angles were allowed to vary within a preset range, typically ±0.05 Å and ±5°. Bond and angle variances and the off-diagonal covariance matrix elements were also allowed to vary in restricted ranges: ±0.005 Å^2, ±50 deg^2, and ±0.5, respectively. The coordination numbers were kept fixed to known crystallographic values. The non-structural parameters in the fits were E_0 (a parameter that aligns the experimental energy scale to the theoretical energy scale), S_0^2 (many-body amplitude reduction factor), Γ_c (core-hole lifetime), and E_r (experimental resolution). These parameters were refined within narrow limits around expected values.[24,25]

(21) (a) Stern, E. A.; Heald, S. M. *Rev. Sci. Instrum.* **1979**, *50*, 1579. (b) Lytle, F. W.; Greegor, R. B.; Sandstrom, D. R.; Marques, E. C.; Wong, J.; Spiro, C. L.; Huffman, G. P.; Huggins, F. E. *Nucl. Instrum. Meth.* **1984**, *226*, 542.

(22) Johansson, L. *Chem. Scr.* **1976**, *9*, 30. The crystal structure of the perchlorate salt has not been determined, but the $[Fe(phenanthroline)_3]^{2+}$ complex structure can be assumed to be identical with that of the corresponding iodide salt (Johansson, L.; Molund, M.; Oskarsson, Å. *Inorg. Chim. Acta* **1978**, *31*, 117).

(23) Mattheiss, L. F. *Phys. Rev.* **1964**, *134*, A970.

Empirical EXAFS Analysis. Data reduction and analysis using empirical phase and amplitude parameters was performed to obtain first shell fits of the Na[Fe(OH_2)EDTA] powder and solution, Na_2[Fe(OH_2)-EDTA] solution, and FeEDTA-NO solution according to the methods described previously[8a,26] and briefly summarized here. A pre-edge subtraction was performed by fitting the EXAFS region with a smooth second order polynomial function which was extrapolated into the pre-edge region and subtracted. A three-segment spline approximately even in k-space with orders of two, three, and three was fit to the EXAFS region and subtracted and the data normalized to an edge jump of one at 7130 eV. The polynomial spline was chosen so that it minimized residual low-frequency noise but did not reduce the amplitude of the EXAFS, as judged by monitoring the FT of the EXAFS as a function of the spline fitting process. The normalized data were converted to k-space. The photoelectron wave vector, k, is defined by $[2m_e(E-E_0)/\hbar^2]^{1/2}$, where m_e is the electron mass, E is the photon energy, $\hbar$ is Planck's constant divided by 2π, and E_0 is the threshold energy of the absorption edge, which was defined to be 7130 eV for the Fe K absorption edge. The empirical EXAFS data analyses were performed with nonlinear least-squares curve-fitting[20,26] techniques using empirical phase and amplitude parameters. The following models were used to obtain the empirical Fe–X backscattering parameters of interest: Fe–O from [Fe(acetylacetonate)$_3$][27] and Fe–N from [Fe(1,10-phenanthroline)$_3$](ClO_4)$_3$.[22]

Fourier transforms (from k to R space) were performed for the data range 3.5–14.5 Å^{-1} with a Gaussian window of 0.1 Å^{-1}. The window widths used in the backtransforms (from R to k space) are presented in the Results and Discussion section. The window widths were kept as similar as possible to the windows used to extract amplitude and phase parameters from the model compounds to minimize artifacts introduced by the Fourier filtering technique. All curve-fitting was based on k^3-weighted data and applied to the individual filtered shell of interest. Only the structure-dependent parameters, the distance and coordination number, were varied. A "goodness of fit" parameter, F, was calculated as $F = \{[k^6(\text{data-fit})^2]/(\text{no. of points})\}^{1/2}$ for each fit.

Results and Discussion

GNXAS Fits of {FeNO}^{7} Complexes with Known Fe–N–O Angles. The GNXAS approach was used to fit the experimental EXAFS data of [Fe(TMC)NO](BF_4)$_2$, Fe(TACN)(N_3)$_2$NO, and Fe(salen)NO at 10 and 220 K. EXAFS contributions for each two-atom and three-atom configuration were calculated using crystallographic distances and bond angles. The individual contributions were then summed to generate a theoretical EXAFS spectrum which was then fit to the non-Fourier filtered experimental EXAFS data without prior background subtraction. In the fits, the crystallographic bond distances and angles were allowed to vary to fit the experimental EXAFS data. A comparison of the theoretical EXAFS spectrum to the experimental data (along with the individual EXAFS signal from each contribution) for each compound is presented in Figures 2–5. A comparison of the bond distances and angles obtained from the GNXAS fits to the crystallographic values is given in Table 1.

The best fit to the EXAFS data of [Fe(TMC)NO](BF_4)$_2$ is presented in Figure 2, with the corresponding FT presented in Figure 6A. The total EXAFS spectrum was accounted for by four contributions: Fe–N(O), Fe–N(TMC), Fe–N–O, and Fe–N–C [throughout this paper, signals from three-atom configurations contain contributions from the three-atom multiple-scattering pathways ($\gamma^{(3)}$ signal) and a two-atom contribution ($\gamma^{(2)}$ signal) from the distant atom[16]]. The GNXAS bond distances and angles match extremely well with the crystallographic values, deviating less than 0.01 Å and 1°, respectively

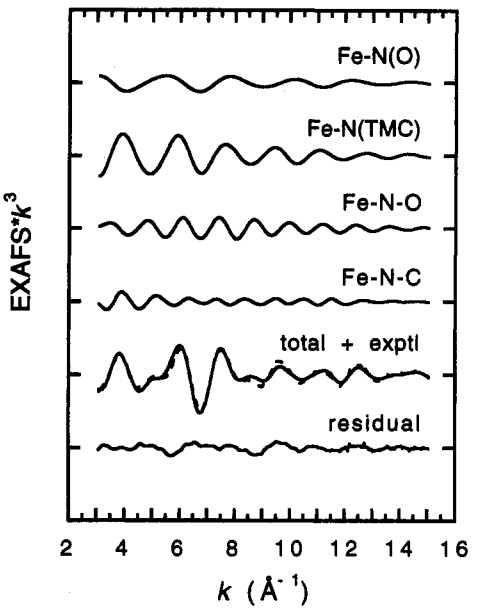

Figure 2. EXAFS signals for individual contributions in the best fit for the [Fe(TMC)NO](BF_4)$_2$ data. The total signal (—) is also shown and compared with the experimental data (- - -) with the residual being the difference between the experimental EXAFS and the theoretical EXAFS. (The ordinate scale is 10 between two consecutive tick marks.) Note the strength of the Fe–N–O contribution.

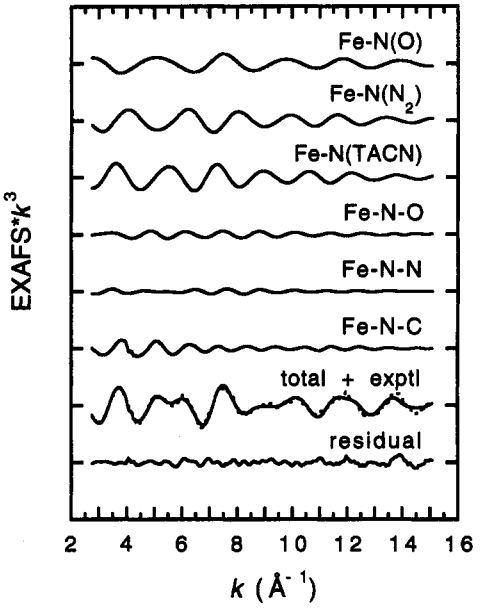

Figure 3. EXAFS signals for individual contributions in the best fit for the Fe(TACN)(N_3)$_2$NO data. The total signal (—) is also shown and compared with the experimental data (- - -) with the residual being the difference between the experimental EXAFS and the theoretical EXAFS. (The ordinate scale is 10 between two consecutive tick marks.)

(Table 1). The linear Fe–N–O multiple-scattering signal is very strong due to the intervening atom focusing effect,[16] allowing for very accurate bond angle determination. The crystallographic Fe–N–O bond angle is 177.5(5)° and the Fe–N–O bond angle obtained from the GNXAS fit is 178°. In the numerous fits that were calculated the bond distances varied by <0.02 Å and the bond angles varied by <1°.

The EXAFS data of Fe(TACN)(N_3)$_2$NO and the best fit to the data are presented in Figure 3 and the FT is shown in Figure 7B. The EXAFS spectrum is dominated by three two-atom signals: Fe–N(O), Fe–N(N_2), and Fe–N(TACN). The significant three-atom signals come from Fe–N–O, Fe–N–N, and Fe–N–C groups. The resultant bond distances and angles are all

(24) Krause, M. O.; Oliver, J. H. *J. Phys. Chem. Ref. Data* **1979**, *8*, 329.
(25) The principal determining factor for E_r is the monochromator and associated vertical slit opening, with the resolution determined by the relationship $\Delta E/E = \cot(\Theta)\Delta\Theta$, where Θ is a function of the Darwin width and the vertical angular acceptance of the monochromator. The values at the Fe K-edge for the experimental conditions used for these experiments were ~1.0–1.5 eV.
(26) (a) Cramer, S. P.; Hodgson, K. O. *Prog. Inorg. Chem.* **1979**, *25*, 1. (b) Scott, R. A. *Methods Enzymol.* **1985**, *117*, 414. (c) Cramer, S. P.; Hodgson, K. O.; Stiefel, E. I.; Newton, W. E. *J. Am. Chem. Soc.* **1978**, *100*, 2748.
(27) (a) Iball, J.; Morgan, C. H. *Acta Crystallogr.* **1967**, *23*, 239. (b) Roof, R. B., Jr. *Acta Crystallogr.* **1956**, *9*, 781.

Table 1. Crystallographic Bond Distances and Angles Compared to GNXAS Results for {FeNO}⁷ Complexes with Known Fe–N–O Angles

compound	structural feature (CN)[e]	GNXAS distance/angle	GNXAS bond variance (σ_R^2)/ angle variance (σ_θ^2)[a]	crystallographic values [range]
$[Fe(TMC)NO](BF_4)_2$	Fe–N (1)	1.73 Å	0.005	1.74 Å
	Fe–N (4)	2.17 Å	0.007	2.16 Å [2.15–2.18]
	N–O (1)	1.14 Å	0.001	1.14 Å
	N–C (4)	1.49 Å	0.004	1.49 Å [1.48–1.50]
	Fe–N–O angle (1)	178.0°	2×10^1	177.5°
	Fe–N–C angle (12)	110.7°	8×10^1	110° [109–114]
$Fe(TACN)(N_3)_2NO$	Fe–N (1)	1.77 Å	0.003	1.74 Å
	Fe–N (2)	2.06 Å	0.004	2.05 Å [2.03–2.08]
	Fe–N (3)	2.25 Å	0.005	2.25 Å [2.24–2.27]
	N–O (1)	1.10 Å	0.001	1.14 Å
	N–N (2)	1.22 Å	0.002	1.19 Å [1.19–1.20]
	N–C (9)	1.43 Å	0.003	1.5 Å [1.4–1.6]
	Fe–N–O angle (1)	156.7°	4×10^0	156°
	Fe–N–N angle (2)	127.7°	3×10^0	124° [121–127]
	Fe–N–C angle (9)	109.0°	8×10^1	108° [104–112]
Fe(salen)NO	Fe–N (1)	1.77 Å	0.006	1.8 Å
10 K[c]	Fe–O (2)	1.87 Å	0.001	1.90 Å [1.87–1.93]
	Fe–N (2)	1.95 Å	0.001	1.97 Å [1.97–1.98]
	N–O (1)	1.16 Å	0.003	1.15 Å[b]
	O–C (2)	1.36 Å	0.003	1.36 Å [1.35–1.37]
	N–C (2)	1.28 Å	0.003	1.28 Å [1.26–1.31]
	N–C (2)	1.49 Å	0.003	1.50 Å [1.49–1.51]
	Fe–N–O angle (1)	131°	1×10^1	127°
	Fe–O–C angle (2)	127°	1×10^0	127° [126–128]
	Fe–N–C angle (2)	124°	1×10^0	124° [123–125]
	Fe–N–C angle (2)	114°	1×10^0	114° [114–115]
220 K[d]	Fe–N (1)	1.76 Å	0.004	1.78 Å
	Fe–O (2)	1.90 Å	0.003	1.91 Å [1.89–1.92]
	Fe–N (2)	2.08 Å	0.012	2.08 Å [2.07–2.08]
	N–O (1)	1.10 Å	0.001	1.11 Å
	O–C (2)	1.31 Å	0.005	1.31 Å [1.30–1.32]
	N–C (2)	1.26 Å	0.004	1.26 Å [1.24–1.27]
	N–C (2)	1.47 Å	0.001	1.45 Å [1.45–1.46]
	Fe–N–O angle (1)	149°	3×10^1	147°
	Fe–O–C angle (2)	132°	3×10^1	130° [126–133]
	Fe–N–C angle (2)	127°	1×10^0	125° [124–126]
	Fe–N–C angle (2)	116°	1×10^1	114° [112–116]

[a] Bond and angle variances are reported in Å² and deg², respectively. [b] Value was fixed in the crystal structure. [c] The crystal structure was determined at −175 °C and the EXAFS was measured at 10 K. [d] The crystal structure was determined at 23 °C and the EXAFS was measured at 220 K. [e] CN = number of configurations in the complex.

within 5% of the crystallographic values (see Table 1) with the Fe–N–O angle equal to 157° (as compared to the crystallographic value of 156(1)°).

The fit to the Fe(salen)NO EXAFS data at 10 K with an Fe–N–O angle of 131° is presented in Figure 4, with the FT of this fit to the data shown in Figure 8C. The two-atom and three-atom contributions included in the fit to the data were Fe–N(O), Fe–O(salen), Fe–N(salen), Fe–N–O, Fe–O–C, and two Fe–N–C signals. The distances and angles obtained from the GNXAS fits were all within 1% of the crystallographic values, Table 1. In the Fe(salen)NO EXAFS data at 10 K the two-atom signals from the O and N of the salen ligand were very strong relative to the signal from the N of the nitrosyl ligand. The bond variances (σ_R^2) are 0.001 Å² for the Fe–O(salen) and Fe–N(salen) contributions and 0.006 Å² for the Fe–N(O) signal. The high bond variance and the associated weak signal for the Fe–N(O) contribution could be due to the fact that the nitrosyl group is disordered.[18] The crystal structure of Fe(salen)NO at −175 °C shows a strongly disordered nitrosyl group with the standard deviation of the Fe–N(O) distance being 0.1 Å and a 1 σ variation of the Fe–N–O angle ranging from 115° to 137°. Not only is the nitrosyl group disordered, but the Fe–N–O angle is below 150.° Significant enhancement of the multiple-scattering signal results when the atoms are arranged in approximately a collinear array, in which case the outgoing photoelectron is strongly forward scattered by the intervening atom. This effect drops off very rapidly for bond angles below ~150°.[6,7,16] Since the Fe–N(O) contribution has a high bond variance and the Fe–N–O angle is low (~130°), the Fe–N–O signal is extremely weak.

The best fit to the Fe(salen)NO EXAFS data at 220 K is presented in Figure 5, with the FT of the best fit to the data shown in Figure 9B. The two-atom and three-atom contributions included in the fit to the data were Fe–N(O), Fe–O(salen), Fe–N(salen), Fe–N–O, Fe–O–C, and two Fe–N–C signals. The distances and angles obtained from the GNXAS fits were all within 1% of the crystallographic values, Table 1. The crystal structure of Fe(salen)NO taken at 23 °C was more accurately determined than the structure at −175 °C, although the oxygen of the nitrosyl group showed some disorder. Two oxygens (OA and OB) were introduced into the crystallographic model with fixed occupancies of 0.5; the Fe–N–OA angle is 144(5)° and the Fe–N–OB angle is 150(4)°. The Fe–N–O angle obtained from the GNXAS fit to the EXAFS data in Figure 5 was 149° with an angle variance of 31 deg², see Table 1. Predictably, the bond variances were higher for the Fe(salen)NO data collected at 220 K, which is also seen in the lower magnitude at high k in the EXAFS data (Figures 4 and 5).

Once best fits were obtained for each {FeNO}⁷ complex, the sensitivity of the fit to the Fe–N–O angle was tested by fixing all the distances, angles, and non-structural parameters and calculating a theoretical EXAFS spectrum with Fe–N–O angles ranging from 90° to 180°. The FTs of relevant calculated spectra for each compound are presented in Figures 6–9. Plots of log(R values) *vs* Fe–N–O angle for each complex are shown in Figure 10 (the log function allows the plots to be scaled for comparison). A minimum in these plots is indicative of a better fit to the experimental EXAFS data.

The FTs of the calculated GNXAS spectra with the Fe–N–O

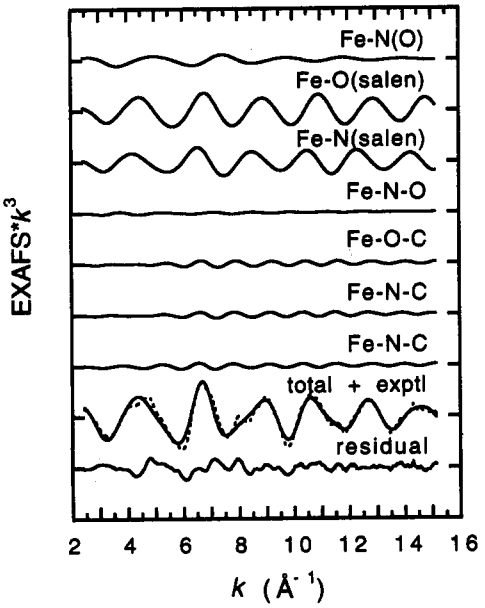

Figure 4. EXAFS signals for individual contributions in the best fit for the Fe(salen)NO at 10 K data. The total signal (—) is also shown and compared with the experimental data (- - -) with the residual being the difference between the experimental EXAFS and the theoretical EXAFS. (The ordinate scale is 10 between two consecutive tick marks.) Note that the Fe–N and Fe–N–O signals are extremely weak.

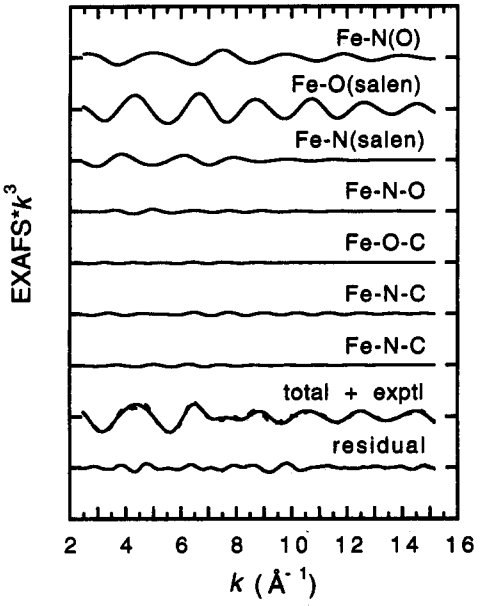

Figure 5. EXAFS signals for individual contributions in the best fit for the Fe(salen)NO at 220 K data. The total signal (—) is also shown and compared with the experimental data (- - -) with the residual being the difference between the experimental EXAFS and the theoretical EXAFS. (The ordinate scale is 10 between two consecutive tick marks.)

angles of 178° (best fit), 150°, and 120° for the [Fe(TMC)NO](BF$_4$)$_2$ data are presented in Figure 6. The second peak in the FT at 2.5 Å, which is due to the Fe–N–O multiple-scattering signal, cannot be accounted for without an Fe–N–O angle that is close to linear. The *R* value dramatically increases in calculated spectra where the Fe–N–O angle is below 170° (Figure 10a). Due to the strength of the multiple-scattering signal from an approximately linear Fe–N–O unit, the calculated spectrum is extremely sensitive to the Fe–N–O angle.

Figure 7 shows the FTs of calculated spectra for Fe(TACN)(N$_3$)$_2$NO with an Fe–N–O angle of 180°, 157° (best fit), and 120°. The FT of the calculated spectrum with Fe–N–O equal to 180° does not match the FT of the experimental EXAFS data.

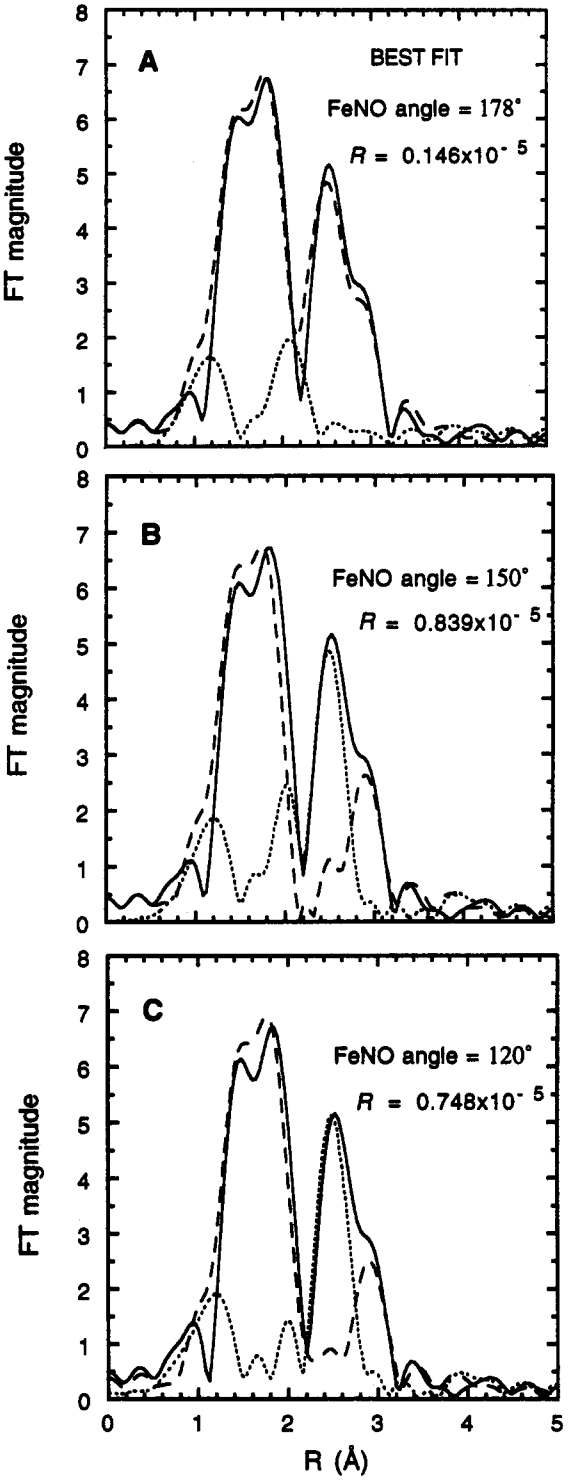

Figure 6. A comparison of the theoretical (- - -) and experimental (—) non-phase shift corrected FT of [Fe(TMC)NO](BF$_4$)$_2$ EXAFS data, along with the FT of the EXAFS residual (···). The *R* value is an indication of the goodness of the fit. Calculated spectra for several different Fe–N–O bond angles are shown: (A) 178° (best fit), (B) 150°, and (C) 120°. This {FeNO}^{7} complex has a crystallographic Fe–N–O bond angle of 177.5(5)°.

When the log(*R* value) is plotted *vs* the Fe–N–O angle there is a minimum between 155° and 160° (Figure 10b) with the crystallographic Fe–N–O angle for Fe(TACN)(N$_3$)$_2$NO being 156°. There is a second shallower minimum in the *R* value at 110°. Upon inspection of the Fe–N–O multiple-scattering signal and the Fe–O (of the Fe–N–O) single-scattering signal, it was observed that in the low *k* region the Fe–O signal with an Fe–N–O angle of 110° was in-phase and of the same order of

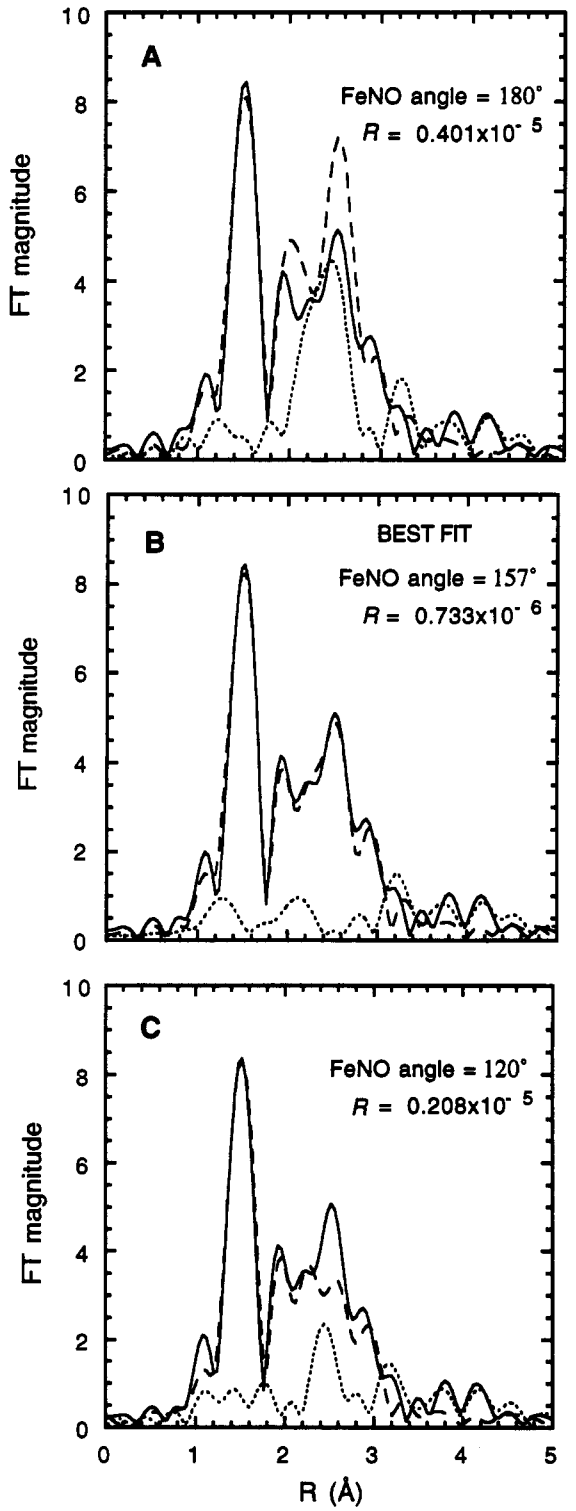

Figure 7. A comparison of the theoretical (- - -) and experimental (—) non-phase shift corrected FT of Fe(TACN)$(N_3)_2$NO EXAFS data, along with the FT of the EXAFS residual (···). The *R* value is an indication of the goodness of the fit. Calculated spectra for several different Fe–N–O bond angles are shown: (A) 180°, (B) 157° (best fit), and (C) 120°. This $\{FeNO\}^7$ complex has a crystallographic Fe–N–O bond angle of 156(1)°.

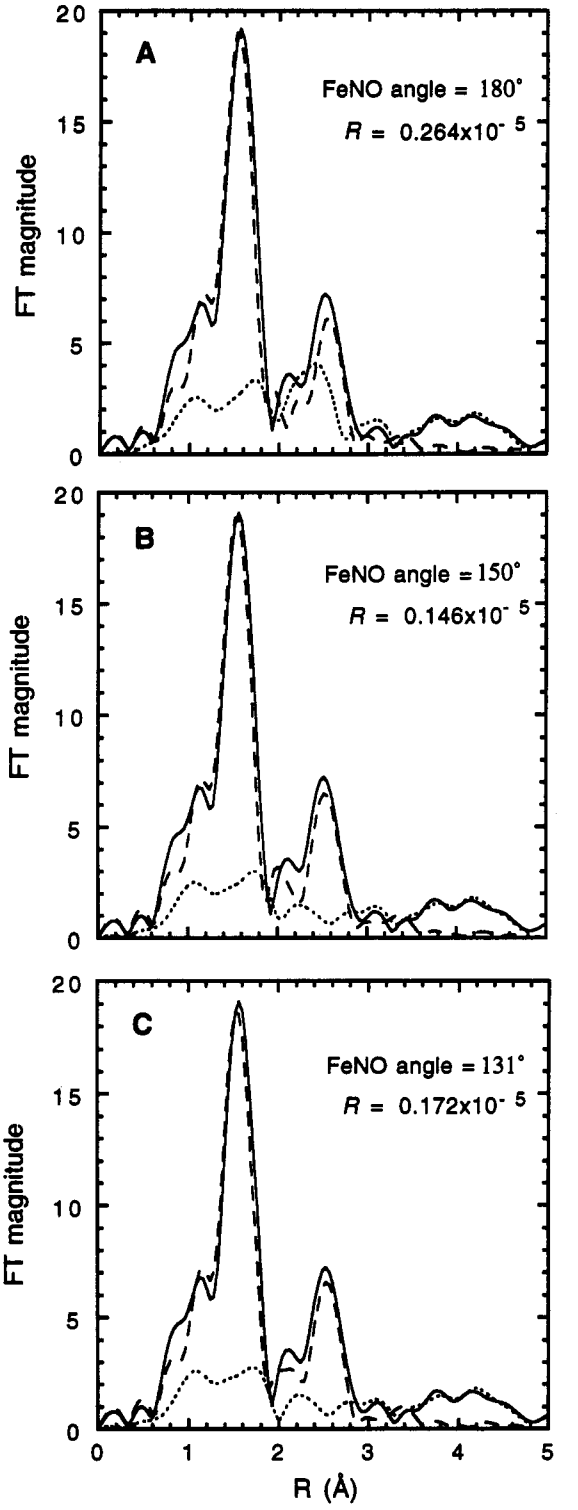

Figure 8. A comparison of the theoretical (- - -) and experimental (—) non-phase shift corrected FT of Fe(salen)NO at 10 K EXAFS data, along with the FT of the EXAFS residual (···). The *R* value is an indication of the goodness of the fit. Calculated spectra for several different Fe–N–O bond angles are shown: (A) 180°, (B) 150°, and (C) 131°. This $\{FeNO\}^7$ complex has a crystallographic Fe–N–O bond angle of 127(6)°. A high Fe–N(O) bond variance made the Fe–N–O signal extremely weak at all angles, even at 180°. Thus, a best fit is not indicated since the GNXAS calculated fits were relatively insensitive to the Fe–N–O angle.

magnitude as the Fe–N–O multiple-scattering signal with an Fe–N–O angle equal to 156°. Therefore the single-scattering Fe–O signal with a Fe–N–O angle of 110° was able to mimic the multiple-scattering Fe–N–O signal with a Fe–N–O angle equal to 156° for *k* less than 6 $Å^{-1}$, giving a false minimum in the log(*R* value) *vs* Fe–N–O angle plot. The multiple-scattering contribution for a three-atom configuration dominates for angles above 150°, while the single-scattering signal is important for values below 150°.[6,7,16] Thus, due to the sinusoidal nature of EXAFS, a double minimum occurs when the log(*R* value) is plotted *vs* the Fe–N–O angle, where in one case the single-scattering signal

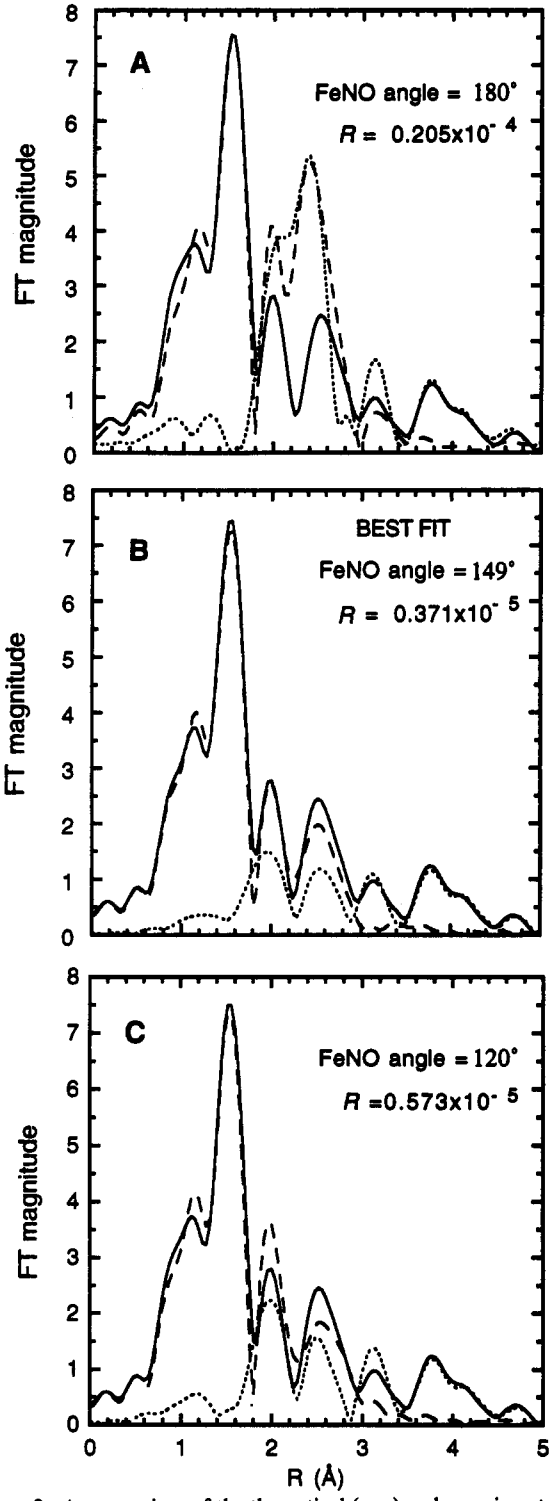

Figure 9. A comparison of the theoretical (- - -) and experimental (—) non-phase shift corrected FT of Fe(salen)NO at 220 K EXAFS data, along with the FT of the EXAFS residual (···). The *R* value is an indication of the goodness of the fit. Calculated spectra for several different Fe–N–O bond angles are shown: (A) 180°, (B) 149° (best fit), and (C) 120°. This model compound has a crystallographic bond angle of 147-(5)°.

(Fe–O) has a phase and amplitude that matches the experimental data and in the other case the multiple-scattering signal (Fe–N–O) has a phase and amplitude that matches the data.

The FTs for calculated spectra of Fe(salen)NO at 10 K with Fe–N–O values of 180°, 150°, and 131° are shown in Figure 8. Since the theoretical spectra were calculated using the bond distances, angles, and the covariance matrix elements of the fit in Figure 4, the bond variance associated with the Fe–N(O) signal

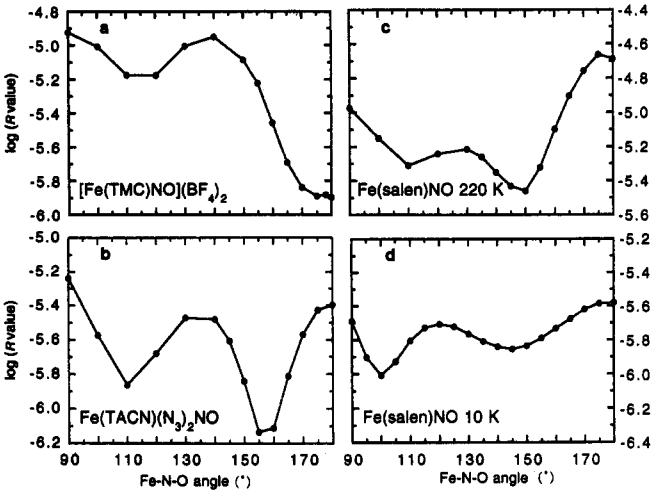

Figure 10. Plots of the log(*R* value) *vs* Fe–N–O angle for (a) [Fe(TMC)NO](BF$_4$)$_2$, (b) Fe(TACN)(N$_3$)$_2$NO, and (c) Fe(salen)NO at 220 K and (d) 10 K where each point represents a match of the calculated EXAFS spectrum to the data. The lower the *R* value the better the fit. The deep minimum in the [Fe(TMC)NO](BF$_4$)$_2$ data at high angles indicates the Fe–N–O angle must be over 170°. The plot for the Fe(TACN)(N$_3$)$_2$NO data has a double minimum with the dominant minimum being around 155°. The minimum in the Fe(salen) 220 K data is at ~150°, while *R* values for the Fe(salen)NO at 10 K were nearly insensitive to variations of the Fe–N–O angle due to the weak Fe–N–O signal.

was very high, 0.006 Å^2. The high Fe–N(O) bond variance made the Fe–N–O signal extremely weak at all angles, even at 180°. Due to the weak Fe–N–O signal, the *R* values of these fits are all very similar and insensitive to the Fe–N–O angle (Figure 10d). Thus, a signal from a three-atom configuration must be a significant component in the total EXAFS signal in order for GNXAS to provide angular information.

The FTs for calculated spectra of Fe(salen)NO at 220 K with Fe–N–O angles of 180°, 149° (best fit), and 120° are shown in Figure 9. Fits above 155° have relatively high *R* values; however, the *R* values for all the fits below 155° are very similar (Figure 10c). In this case, application of GNXAS to the data only allows an upper limit of 155° to be set for the Fe–N–O angle.

Fe–N–O Angle Determination of an {FeNO}^{7} Complex of Unknown Structure. GNXAS analysis was used to investigate the Fe–N–O angle of FeEDTA-NO, a complex whose structure is unknown. GNXAS requires an initial structural model. Therefore, EXAFS data of several FeEDTA complexes were obtained and compared to FeEDTA-NO to determine a suitable initial structural model. With use of the empirical EXAFS data analysis method, first shell distances were obtained for Na[Fe(OH$_2$)EDTA] powder, Na[Fe(OH$_2$)EDTA] solution, Na$_2$[Fe(OH$_2$)EDTA] solution, and FeEDTA-NO solution. The EXAFS of both the powder and solution forms of Na[Fe(OH$_2$)EDTA] were studied to determine if there is any significant structural change between solid and solution forms. The results of the first shell empirical fits are given in Table 2 and Figure 11.

The first shell distances obtained from the best fit, Fit #1, to the Na[Fe(OH$_2$)EDTA] powder data match extremely well to the crystallographic values of Li[Fe(OH$_2$)EDTA]·2H$_2$O[19] (Table 3) with two shells of O at ~2.0 and ~2.1 Å and 2 N at ~2.3 Å. The first shell distances obtained from the best fit, Fit #2, to the Na[Fe(OH$_2$)EDTA] solution data are very similar to those of the powder sample. The shorter Fe–O distance was elongated by 0.02 Å in the solution sample and the coordination numbers were slightly different. It appears that there are no major changes in the first shell of the Na[Fe(OH$_2$)EDTA] structure between the solution and the powder since both the difference in the short Fe–O distance and the differences in the coordination numbers are within the uncertainty of the technique. The first shell

Table 2. First Shell Empirical Fits of FeEDTA Complexes

sample	fit no.	FT window width (Å)	element	CN[a]	bond length (Å)	F[b]
$Na[Fe(OH_2)EDTA]$ (powder)	#1	[0.8–2.2]	O	2.5	1.98	0.40
			O	2.5	2.12	
			N	1.8	2.34	
$Na[Fe(OH_2)EDTA]$ (solution)	#2	[0.8–2.2]	O	2.7	2.00	0.40
			O	1.6	2.12	
			N	1.6	2.34	
$Na_2[Fe(OH_2)EDTA]$ (solution)	#3	[1.0–2.2]	O	3.4	2.17	0.46
			N	1.9	2.34	
FeEDTA-NO (solution)	#4	[1.1–2.0]	N	1.1	1.76	0.39
			O	3.2	2.05	
			N	1.5	2.27	
	#5		O	3.5	2.06	0.85
			N	1.9	2.28	

[a] CN = coordination number. [b] $F = \{[k^6(\text{data-fit})^2]/(\text{no. of points})\}^{1/2}$.

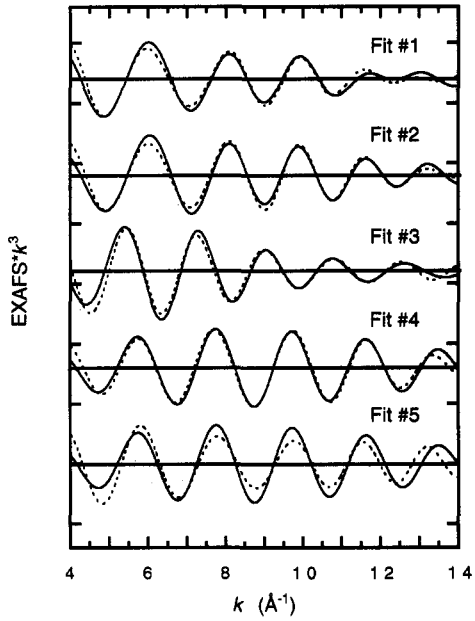

Figure 11. Empirical first shell fits to the Fourier-filtered EXAFS data with the solid line representing the experimental data and the dashed line representing the fit to the data. Fits #1, #2, and #3 are the best empirical fits to the $Na[Fe(OH_2)EDTA]$ powder data (Table 2), to the $Na[Fe(OH_2)EDTA]$ solution data, and to the $Na_2[Fe(OH_2)EDTA]$ solution data, respectively. Fits #4 and #5 are fits to the FeEDTA-NO data with Fit #4 containing a short Fe–N distance. (The ordinate scale is 5 between consecutive tick marks with solid horizontal lines going through the zero point of each plot.)

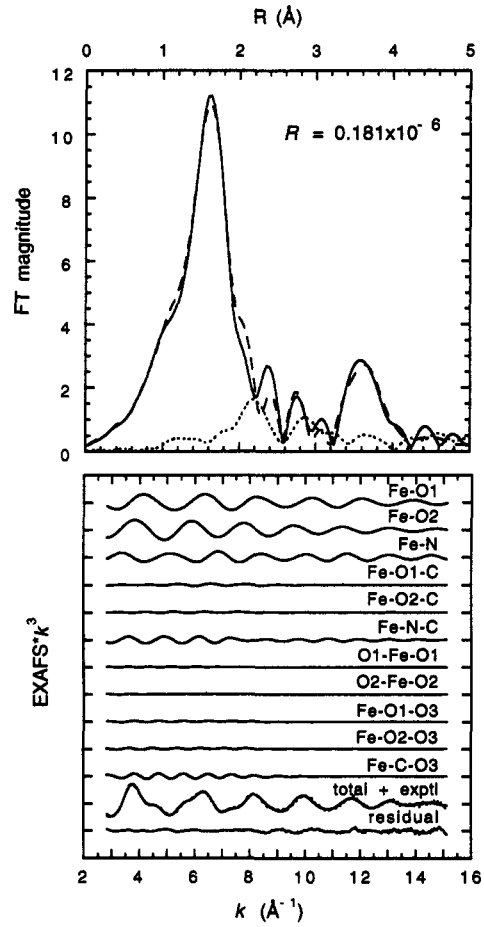

Figure 12. Comparison of the GNXAS theoretical signal with the experimental data of Fe K-edge k^3-weighted EXAFS of $Na[Fe(OH_2)EDTA]$ solution data. The top portion of the figure contains the non-phase shift corrected FT of the k^3-weighted EXAFS data of the experimental data (—) and that of the total theoretical signal (- - -). Also shown is the FT of the residual (···). The lower portion of the figure presents the EXAFS signals for the individual contributions. The total theoretical signal is also shown (—) and compared with the experimental data (···) with the residual being the difference between the experimental EXAFS and the theoretical EXAFS. (The ordinate scale is 10 between two consecutive tick marks.)

distances obtained from the best fit, Fit #3, to the $Na_2[Fe(OH_2)EDTA]$ EXAFS data are given in Table 2. While the presence of two shells of O could not be resolved in the reduced form, an average distance of 2.17 Å was obtained which is 0.12 Å longer than the average Fe–O distance in $Na[Fe(OH_2)EDTA]$.

Two fits (Fits #4 and #5) are shown (Figure 11) for the FeEDTA-NO solution, one fit with and one without a short Fe–N bond from the Fe–N–O unit. Fit #4, which includes the short Fe–N bond, is substantially better than Fit #5, without the short Fe–N bond, with the F value being over a factor of 2 lower for Fit #4. The best fit to the FeEDTA-NO data has 1.1 N at 1.76 Å, 3.2 O at 2.05 Å, and 1.5 N at 2.27 Å. The short 1.76 Å Fe–N distance is typical for the $\{FeNO\}^7$ systems.[4] The Fe–O distance appears to be an average of two Fe–O shells, which could not be resolved given the range of available data. A fit with four contributions was attempted (Fe–N at ~1.8 Å, Fe–O at 2.0 Å, Fe–O at ~2.1 Å, and Fe–N at ~2.3 Å) but both Fe–O distances coalesced at 2.05 Å with an F value identical to that for Fit #4.

The Fe–O and Fe–N distances of the EDTA ligand in FeEDTA-NO are more similar to the respective distances in $Na[Fe(OH_2)EDTA]$ than those in $Na_2[Fe(OH_2)EDTA]$. In addition, the XAS edge of FeEDTA-NO is more similar to the edge of $Na[Fe(OH_2)EDTA]$ than to that of $Na_2[Fe(OH_2)EDTA]$.[5] The coordination number of the oxygens varies in a chemicallyreasonable way for the solid $Na[Fe(OH_2)EDTA]$, solution $Na[Fe(OH_2)EDTA]$, and FeEDTA-NO. The crystallographically-characterized $[Fe(OH_2)EDTA]^-$ has 5 oxygens in the first shell and the best fits to the $Na[Fe(OH_2)EDTA]$ powder and solution data give an oxygen coordination number of 5.0 and 4.3, respectively. The somewhat lower coordination number in solution

Table 3. Comparison of the $Li[Fe(OH_2)EDTA]\cdot 2H_2O$ Crystallographic Bond Distances and Angles to the GNXAS and Empirical Fitted Bond Distances and Angles for $Na[Fe(OH_2)EDTA]$ Solution and Powder and FeEDTA-NO

		$Na[Fe(OH_2)EDTA]$ powder			$Na[Fe(OH_2)EDTA]$ Solution			FeEDTA-NO Solution		
structural feature (CN)[a]	$Li[Fe(OH_2)EDTA]\cdot 2H_2O$ crystallographic values [range]	GNXAS distances/ angles	GNXAS variances[b]	empirical first shell distances	GNXAS distances/ angles	GNXAS variances[b]	empirical first shell distances	GNXAS distances/ angles	GNXAS variances[b]	empirical first shell distances
$Fe-O_1$ (2)	1.97 Å [1.94–2.00]	1.97 Å	0.003	1.98 Å	1.98 Å	0.003	2.00 Å	2.03 Å	0.002	2.05 Å[d]
$Fe-O_2$ (3)	2.11 Å [2.11–2.13]	2.10 Å	0.004	2.12 Å	2.09 Å	0.006	2.12 Å	2.11 Å[c]	0.006[c]	
Fe–N (2)	2.32 Å [2.30–2.35]	2.33 Å	0.003	2.34 Å	2.35 Å	0.002	2.34 Å	2.33 Å	0.010	2.27 Å
O_1-C (2)	1.28 Å [1.27–1.29]	1.33 Å	0.005		1.33 Å	0.006		1.29 Å	0.004	
O_2-C (2)	1.26 Å [1.26–1.27]	1.30 Å	0.004		1.30 Å	0.005		1.31 Å	0.005	
N–C (6)	1.47 Å [1.47–1.48]	1.48 Å	0.002		1.47 Å	0.002		1.47 Å	0.003	
$O_{1,2}-O_3$ (4)	2.23 Å [2.20–2.25]	2.30 Å	0.006		2.27 Å	0.006				
$C-O_3$ (4)	1.23 Å [1.21–1.25]	1.27 Å	0.002		1.28 Å	0.007		1.29 Å	0.008	
Fe–C (4)	2.90 Å [2.79–2.99]	2.91 Å	0.008		2.92 Å	0.008		2.96 Å	0.010	
Fe–N (1)								1.78 Å	0.003	1.76 Å
N–O (1)								1.10 Å	0.001	
Fe–N–O angle (1)								156°	2×10^0	
$Fe-O_1-C$ angle (2)	120° [119–121]	121°	3×10^1		123°	3×10^1		122°	3×10^1	
$Fe-O_2-C$ angle (2)	122° [121–123]	119°	6×10^1		124°	6×10^1		122°	6×10^1	
Fe–N–C angle (6)	108° [103–112]	106°	1×10^1		106°	1×10^1		104°	6×10^1	
O_1-Fe-O_1 angle (1)	166°	170°	7×10^0		170°	1×10^1				
O_2-Fe-O_2 angle (1)	145°	150°	2×10^0		150°	2×10^0				
$Fe-O_1-O_3$ angle (2)	145° [142–148]	150°	5×10^1		150°	5×10^1				
$Fe-O_2-O_3$ angle (2)	149° [148–150]	155°	5×10^1		155°	6×10^1				
$Fe-C-O_3$ angle (4)	158° [153–161]	158°	1×10^1		159°	1×10^1		158°	2×10^1	

[a] CN = number of configurations in the complex. [b] Bond variances (σ_R^2) and angle variances (σ_θ^2) are reported in $Å^2$ and deg^2, respectively. [c] Coordination number was fixed at 2. [d] Average of both Fe–O shells.

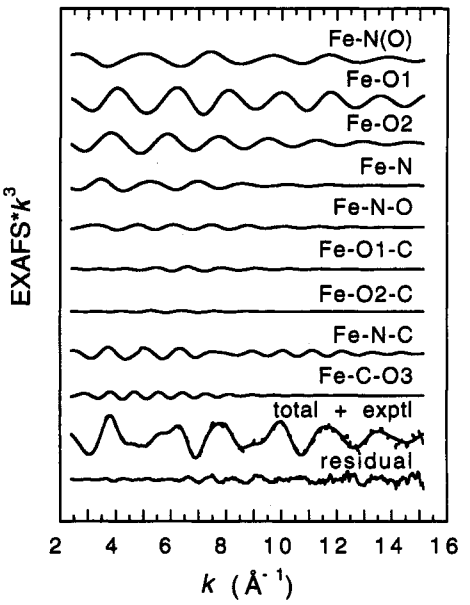

Figure 13. EXAFS signals for individual contributions in the best fit for the FeEDTA-NO data. The total signal (—) is also shown and compared with the experimental data (- - -) with the residual being the difference between the experimental EXAFS and the theoretical EXAFS. (The ordinate scale is 10 between two consecutive tick marks.)

could be related to an increased disordered in the solution. The NO seems to take the place of the H_2O at 2.11 Å, since the oxygen coordination number has decreased to 3.2 in the best FeEDTA-NO fit.

The GNXAS approach was used to analyze EXAFS data of $Na[Fe(OH_2)EDTA]$ powder and solution to ensure that the MS contributions could be properly accounted for and that reliable second and third shell bond distances and bond angles could be obtained. The results of the fits to the $Na_2[Fe(OH_2)EDTA]$ solution data also provided values for bond and angle variances and the off-diagonal covariance matrix elements for the fits to the FeEDTA-NO data.

The best fit to the $Na[Fe(OH_2)EDTA]$ powder data will be presented and discussed elsewhere.[16] The low-frequency EXAFS is dominated by three waves from two-atom contributions: $Fe-O_1$, $Fe-O_2$, and Fe–N, where O_1 refers to the oxygen at 1.97 Å and O_2 refers to the oxygen at 2.11 Å. The EXAFS distances for these three shells show excellent agreement with the crystallographic values of the $Li[Fe(OH_2)EDTA]\cdot 2H_2O$,[19] deviating by <0.01 Å (Table 3). There were approximately 30 unique three-atom configurations which ranged in distance from 3.0 to 4.5 Å. The eight main contributions were from $Fe-O_1-C$, $Fe-O_2-C$, Fe–N–C, O_1-Fe-O_1, O_2-Fe-O_2, $Fe-O_1-O_3$, $Fe-O_2-O_3$, and $Fe-C-O_3$, where O_3 refers to the oxygen outside the first shell. The GNXAS determined bond distances and angles that make up the three-atom contributions are within 5% of the crystallographic values, with the strength of the signal influencing the goodness of the match.[16] Contributions with stronger signals have distances and angles that match closer to the crystallographic values than do contributions with weaker signals. Over a large number of fits with varying contributions, splines, and non-structural parameters the first shell distances varied by <0.01 Å, the low Z bond distances (*i.e.* O–C and N–C) varied by ±0.04 Å, and the bond angle varied by ±3°. The GNXAS first shell distances are within 0.02 Å of the empirical first shell distances, with the GNXAS distances being slightly closer to the crystallographic values.

The EXAFS data and the FT of the best fit to the $Na[Fe(OH_2)EDTA$ solution data are presented in Figure 12 and the bond distances and angles from that fit are given in Table 3. The main contributions to the EXAFS are the same as for the $Na[Fe(OH_2)EDTA]$ powder. The best fit shows excellent agreement with the experimental EXAFS as does the FT of the experimental data and the fit. The bond distances obtained from the best fit to the $Na[Fe(OH_2)EDTA]$ solution data are within 0.02 Å of the $Na[Fe(OH_2)EDTA]$ powder values and the bond angles are all within 2° with two exceptions. There is a 0.03 Å difference in the $O_{1,2}-O_3$ distance and a 5° difference in the $Fe-O_2-C$ angle. However, both the $O_{1,2}-O_3$ distance and the $Fe-O_2-C$ angle show large disorder, with a bond variance of 0.006 $Å^2$ and an angle variance of 60 deg^2 (Table 3). The bond and angle variances are very similar, but slightly larger than the powder values, which is expected since there should be more disorder in solution. The increase in the solution variances is also consistent with the fact that in the empirical analysis (where the Debye–Waller factors are fixed) the coordination numbers for the solution were lower than those of the powder. The similarities in bond lengths, bond angles, and the respective variances indicate that the $[Fe(OH_2)-EDTA]^-$ unit is structurally the same in the powder and the

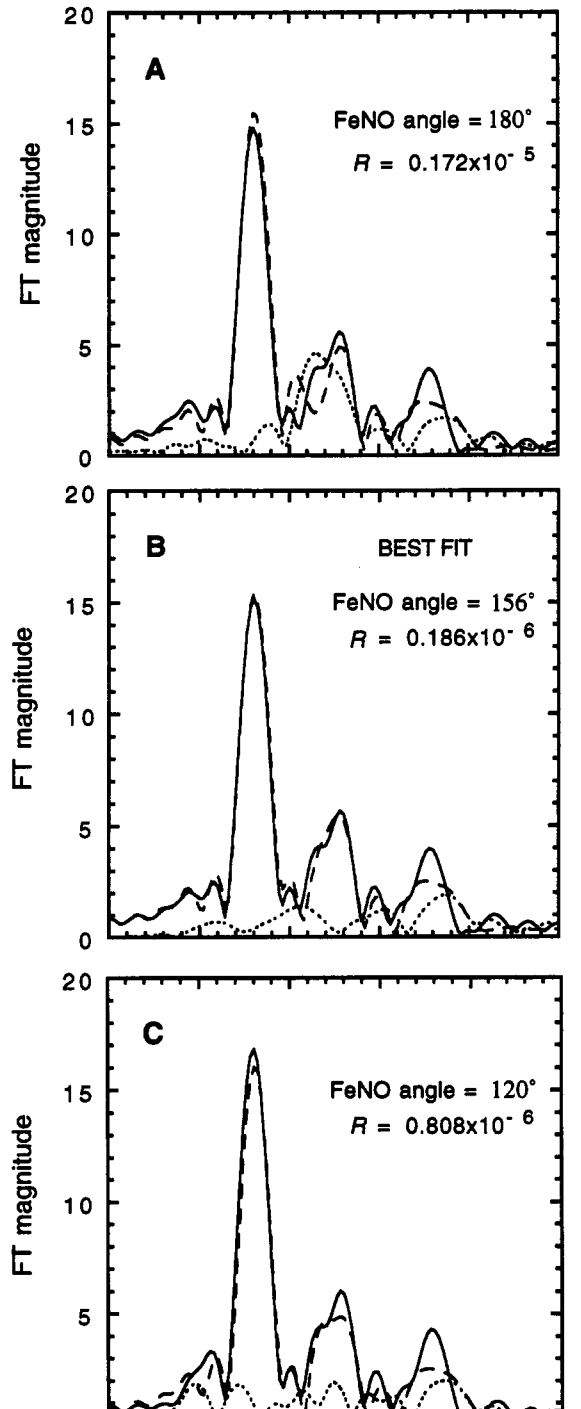

Figure 14. A comparison of the theoretical (- - -) and experimental (—) non-phase shift corrected FT of FeEDTA-NO EXAFS data, along with the FT of the EXAFS residual (···). The *R* value is an indication of the goodness of the fit. Calculated spectra are for Fe–N–O bond angles of (A) 180°, (B) 156° (best fit), and (C) 120°.

solution form. Therefore it is a reasonable approximation to initially model FeEDTA-NO in the solution form using the crystallographic coordinates of $Li[Fe(OH_2)EDTA]\cdot 2H_2O$ with NO replacing the H_2O.

The best fit to the EXAFS of the FeEDTA-NO solution data is shown in Figure 13 and the bond distances and angles are presented in Table 3. The FT of the EXAFS data of the best fit is shown in Figure 14B. The initial $[Fe(OH_2)EDTA]^-$ structural model was modified by including a short Fe–N distance

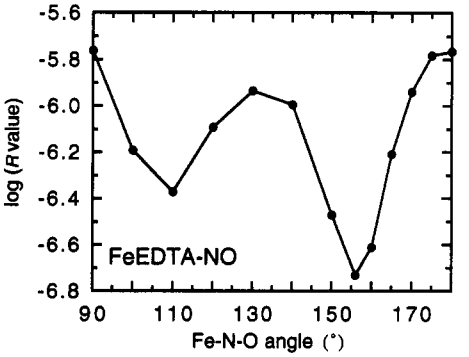

Figure 15. Plot of the log(*R* value) *vs* Fe–N–O angle for FeEDTA-NO where each point represents a match of the calculated EXAFS spectrum to the data. The lower the *R* value the better the fit. This plot of FeEDTA-NO calculated spectra exhibits similar behavior to the plot of the Fe(TACN)$(N_3)_2$NO calculated spectra (Figure 10b) with the dominant minimum being around 155°.

(~1.8 Å) and fixing the coordination number for the 2.1 Å Fe–O distance at two. Fits were done using $\gamma^{(2)}$ signals exclusively to determine first shell distances. Once a reasonable fit was obtained, the first shell distances were fixed and a Fe–N–O signal was added to the fit. Fe–N–O signals were calculated every 10° between 90° and 180°, fixing the Fe–N distance at 1.8 Å and the N–O distance at 1.1 Å. Fits were then performed including the Fe–N–O signal at each angle. Reasonable fits were obtained for Fe–N–O angles between 150° and 160°. At this point, other three-atom signals were included in the fits allowing the distances, angles, and elements of the covariance matrix to vary within a restricted range. The Fe–N–O angle was allowed to vary between 145° and 165°. Several of the three-atom contributions included in the fit to the $Na[Fe(OH_2)EDTA]$ solution data (Figure 12) were left out of the FeEDTA-NO fits (O_1–Fe–O_1, O_2–Fe–O_2, Fe–O_1–O_3, and Fe–O_2–O_3), since the signals were relatively weak and only increased the number of variables in the fit. The distances and bond angles obtained from the GNXAS final fit are very similar to the distances and bond angles from the GNXAS fits of the $Na[Fe(OH_2)EDTA]$ powder and solution data as can be seen in Table 3. The complicated EXAFS data in Figure 13 are dominated by four waves of lower frequency: Fe–N(O), Fe–O_1, Fe–O_2, and Fe–N. However, the longer Fe–N contribution is much weaker than in the $Na[Fe(OH_2)EDTA]$ powder and solution EXAFS with a bond variance that is three to four times higher indicating that the bond between the Fe–N at ~2.3 Å may be weakened when the NO binds. The Fe–N–O signal is fairly strong compared to the other three-atom signals. The Fe–N(O) and N–O bond distances obtained from the GNXAS fit were 1.78 and 1.10 Å, respectively. These distances are consistent with other Fe–N(O) and N–O bond distances in {FeNO}⁷ systems.[4] A fit with an Fe–N–O angle of 156° shows excellent agreement with the experimental EXAFS data, Figure 13, and with the Fourier transformed data, Figure 14B, up to 3.5 Å. The discrepancy between the theoretical and experimental signal in the FT beyond 3.5 Å can be attributed to the fact that several three-atom contributions associated with weaker signals in that region were not included in the fit.

As was done with the crystallographically-characterized {FeNO}⁷ complexes, the sensitivity of the calculated spectrum to the EXAFS data for FeEDTA-NO was tested as a function of Fe–N–O angle. The FTs for FeEDTA-NO with Fe–N–O values of 180°, 156° (best fit), and 120° are shown in Figure 14. A plot of log(*R* value) *vs* Fe–N–O angle (Figure 15) of the FeEDTA-NO data displays a minimum at 156°. This looks extremely similar to the plot of the Fe(TACN)$(N_3)_2$NO data, where Fe(TACN)$(N_3)_2$NO has an Fe–N–O angle of 156°. It is not surprising that the geometric structures of the Fe–N–O unit in

$Fe(TACN)(N_3)_2NO$ and FeEDTA-NO are similar since both compounds exhibit very similar optical spectroscopy.[5,28]

Summary

Multiple-scattering signals from three-atom configurations are accurately modeled by GNXAS to obtain angular information on the Fe–N–O unit of $\{FeNO\}^7$ complexes. The GNXAS fits to the $\{FeNO\}^7$ model compounds are sensitive to the Fe–N–O angle when the Fe–N–O signal is significant in comparison with the total EXAFS signal. It is possible to determine whether the Fe–N–O unit is linear or bent and estimate the Fe–N–O angle, with the GNXAS fits being very sensitive when the angle is between 150° and 180°. The Fe–N–O angle of a crystallographically-uncharacterized $\{FeNO\}^7$ model complex was determined. Using this method the Fe–N–O angle of FeEDTA-NO is determined to be bent, and close to 156°. The results of this study establish that EXAFS analysis using GNXAS can provide reliable angular information on low Z small molecules liganded to transition metal complexes. This work provides the basis for studying NO complexes with transition metal active sites in metalloproteins. It is also straightforward to extend this methodology to study other diatomics such as O_2^- or O_2^{2-} liganded to transition metal sites.

(28) Zhang, Y.; Pavlosky, M. A.; Brown, C. A.; Westre, T. E.; Hedman, B.; Hodgson, K. O.; Solomon, E. I., to be submitted for publication.

Acknowledgment. The $Na[Fe(OH_2)EDTA]$, $Na_2[Fe(OH_2)$-EDTA], and FeEDTA-NO solutions were prepared and provided by Y. Zhang and M. Pavlosky. This research was supported by grants from the NIH (RR01209, K.O.H.; GM40392, E.I.S) and NSF (CHE91–21576, K.O.H.) and also the Italian INFN and CNR research institutions. The Stanford Synchrotron Radiation Laboratory is supported by the Department of Energy, Office of Basic Energy Sciences, Divisions of Chemical Science and Material Science, and in part by the National Institutes of Health, National Center of Research Resources, Biomedical Research Technology Program and DOE's Office of Health and Environmental Research.